92

UO_2 – Zr CHEMICAL INTERACTION OF PHWR FUEL PINS UNDER HIGH TEMPERATURE

P. MAJUMDAR, D. MUKHOPADHYAY, S. K. GUPTA

Reactor Safety Division, Bhabha Atomic Research Center
Mumbai 400 085, India - E-mail: dmukho@apsara.barc.ernet.in

Keywords : Severe accident, Fuel heat up, Pellet-clad-steam interaction

At high temperature Zircaloy clad interacts with the UO_2 fuel as well as with the steam to produce oxide layer of α-Zr(O) and ZrO_2. This layer formation significantly reduces the structural strength of the clad. A computer code 'SFDCPA/MOD1' has been developed to simulate the interaction and predict the oxide layer thickness for any accidental transient condition. It is well validated with published experimental data on the isothermal and transient temperature condition. The program is applied to Indian Pressurized Heavy Water Reactor (PHWR) fuel pin under certain severe transient condition where it experiences temperature above 1000^{O}C. The study gives an idea of the un-oxidized thickness of Zircaloy, which is an important criterion for fuel integrity.

INTRODUCTION

In Indian Pressurized Heavy Water Reactor (PHWR), Loss of Coolant Accident along with failure of Emergency Core Cooling System (ECCS) would heat up the fuel and clad to very high temperature. It initiates a chemical interaction between pellets and clad along with clad interaction with steam at the external surface. This paper deals with the development of a Severe Fuel Damage and Consequent Problem Analysis (SFDCPA/MOD1) code, which presently simulates the fuel - clad - steam interaction in the temperature range of 820^{O}C - 1750^{O}C and its application to Indian PHWR fuel pin. At high temperature, the fuel - clad element is subjected to both internal and external oxidation. This interaction is exothermic, which escalates the process further. The external oxidation, i.e. Zircaloy and coolant interaction, were studied by many authors and number of codes were developed to simulate the reaction kinetics. The chemical interaction between UO_2 and Zr, at the inner boundary of clad, is well established by experiments conducted by Cronenberg (1978), Olander (1983) and Hofmann (1984). Theoretical simulation of chemical kinetics of reaction layer formation and growth has seen two approaches. Isothermal experiments revealed that growth of various phases follows parabolic rate law. Arrhenius equation as a function of time and temperature for each of the interface were formulated with experimentally found constants. However, this approach was found to fail in certain temperature transients and for longer annealing time as each phase starts attaining

saturation. In the other approach diffusion models were applied to analyze the problem. The model is based on the solution of Fick's and Stefan's equation. The code SFDCPA adopts Hofmann model (1988), which solves diffusion equation in the phases for oxygen distribution and Stefan's equation at the interfaces. It uses the method of finite difference in each phase with its boundary moving with time. The results are validated with experimental data available in the literature both for transient and isothermal conditions.

Indian PHWR fuel pins are having collapsible clad which aggravates the possibility of internal interaction. SFDCPA / MOD1 has been used for prediction of such chemical interaction during heat up of the fuel pins. The accident condition has been simulated using RELAP4/MOD6 (Fischer, 1978). During heat up, the fuel pins balloon and contact each other. This causes steam starvation at the contact point and influences the oxide layer growth. Therefore, separate simulation has been carried out at steam availability and non-availability condition.

INDIAN PHWR SYSTEM

The configuration of 220 MWe Indian PHWR and its fuel pin are described in this section. The reactor core, where fission chain reaction takes place and energy is generated, consists of an array of horizontal reactor channels (306 in number) housed in a cylindrical vessel called calandria. Each reactor channel consists of Pressure Tubes and Calandria tubes. The pressure tube contains 12 fuel bundles (495mm long), which are cooled by pressurized heavy water at a mean temperature of 271°C (inlet 249°C and outlet about 293°C) and at average pressure of 90 bar. Each fuel bundle has 19 rods and is supported by End Plates at both the ends. Cross section of a reactor channel is shown in Fig.1. The calandria is filled with heavy water, which act as a moderator. It is maintained at an average temperature of about 60°C. Moderator is separated from the hot reactor coolant by the calandria tubes and the pressure tubes with annuli gas space in between them. Each fuel pin consists of 24 pellets and sheathed with Zircaloy clad, which remain intact with pellet under normal operating condition.

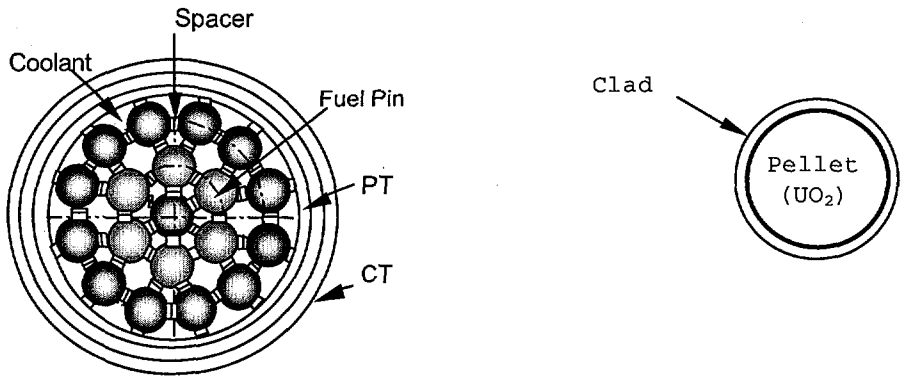

Fig.1 Reactor channel configuration

UO2 / Zr REACTION KINETICS

The reaction of UO2 with Zirconium and Zircaloy–2 were studied systematically by Malett et al. (1957) and by Grossman and Rooney (1965) at temperature up to 1200^{O}C. Hofmann and Politis (1979) performed out of pile experiment with UO_2 and Zr–4 between 900^{O}C and 1500^{O}C. More recently, Hofmann and Kerwin Peck (1984) conducted experiments with UO_2 and Zry-4 for temperature ranging from 1000^{O}C to 1700^{O}C. Results were obtained for both isothermal and transient temperature with over pressure of 1 bar and 80 bar. The equilibrium phases of the (U – Zr – O) ternary system have been studied by Politis (1975).

During normal operating condition, the temperature range is such that fuel – clad remain intact and Zircaloy clad exists in the Hexagonal Closed Packed structure (α-phase). A rise in temperature initiates both external oxidation (metal – steam reaction) and internal oxidation (UO_2–Zr interaction) of Zircaloy clad. Oxygen affinity of Zirconium is the driving force of the reaction. External oxidation, when sufficient steam exists, involves the formation of ZrO_2 beneath which oxygen stabilised α–Zr is produced. At the core, β–Zr is formed at high temperature. It is found that when sufficient contact exists, chemical interaction between UO_2 and Zr is circumferentially and axially very uniform. Zircaloy reduces UO_2 to form oxygen stabilised α–Zr(O) and uranium metal. The metallic uranium then reacts with zirconium to form an eutectic layer (U-Zr) between two oxygen stabilised α-Zr(O) layers. U-Zr has low melting point around 1150^{O}C depending on Zr-content. Therefore the sequence of layer formed during initial temperature condition (>1000^{O}C) is as below.(Fig.2)

$[UO_2+U]$ (I) $\rightarrow$ [α-Zr(O)$_a$ + (U-Zr)](II) $\rightarrow$ (U -Zr)alloy (III) $\rightarrow$ α-Zr(O)$_b$ (IV) $\rightarrow$ β-Zry (V) $\rightarrow$ α-Zr(O)$_c$(VI) $\rightarrow$ ZrO_2(VII)

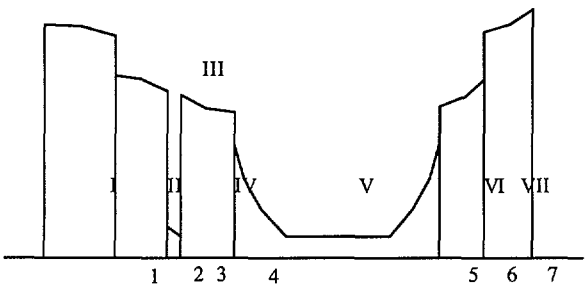

Fig. 2 Layer positions of the system

Phase–II consists of radially elongated α-Zr(O) grain with small amount of U-Zr along the grain boundaries. Oxygen is removed from phase-I until the oxide reaches lower phase boundary. Oxygen diffuses through phase-II, phase-III and reaches phase-IV. The oxygen solubility of layer-III is very low (0.3 wt%), hence it does not retain any oxygen atom diffusing in it. The liquid (U-Zr) alloy may flow along axial direction and through cracks. Hence the boundary is not well defined. This layer no longer remains in closed form for higher annealing time. It changes to discontinuous globules and mixes with α-Zr(O) layers.

The uranium atom, formed by the reduction of UO_2, also diffuses along with the oxygen. However, no uranium atom is detected in layer-IV and layer-V. Zirconium atom diffuses in opposite direction. As oxidation progresses, the β-phase tends to vanish. The phases α-$Zr(O)_b$ and α-$Zr(O)_c$ merge into a single phase. Later on, the layer α-Zr(O) and (U-Zr) also disappears and ZrO_2 and UO_2 remain. The above complete progress is only observed at higher annealing time. It is observed that these layers grow parabolically with time at early stage, but growth is stopped after the clad is saturated with oxygen.

MATHEMATICAL FORMULATION

Both external and internal oxidation are primarily oxygen diffusion controlled and the present model does not take into account uranium and zirconium diffusion. The SFDCPA model is based on the solution of linearized diffusion (Fick's) equation for oxygen at each of the experimentally observed layer. The growth of each layer is calculated from the principle of oxygen mass conservation at the layer boundary.
Neglecting the effect of zirconium lattice movement on oxygen diffusion. Fick's equation can be written as

$$\frac{\partial C}{\partial t} = \nabla^2 C \qquad [1]$$

As mentioned earlier when sufficient contact exists, the interaction is circumferentially uniform. Hence, it is sufficient to formulate the problem in 1-D. Eq-1 can be simplified in cylindrical form as below,

$$\frac{\partial C}{\partial t} = D\frac{\partial^2 C}{\partial r^2} + \frac{D}{r}\frac{\partial C}{\partial r} \qquad [2]$$

The oxygen in the fuel is assumed to be loosely bound to the uranium oxide molecule so that oxygen movement is solely governed by its concentration gradient. Since the difference in the incoming and outgoing fluxes (Fig.3) give rise to interface movement the Stefan's equation can be written as follows,

$$\ddot{A}C\frac{dx}{dt} = J_{in} - J_{out} \qquad [3]$$

where, oxygen flux, $J = -D\frac{dC}{dr}$ [4]

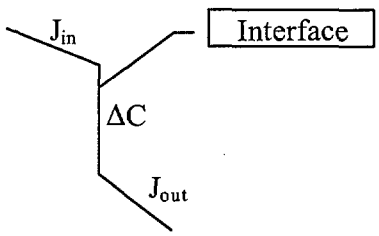

Fig.3 Fluxes at phase boundaries

The difference in the oxygen atom flow is basically consumed in the formation of oxide layer. Interface moves because of finite concentration difference at the interface and concentration gradient in the adjacent phases. The boundary concentrations are defined by the phase diagram at equilibrium conditions. Apart from interface movements, because of concentration difference, volumetric

expansion and contraction occurs within the phase and a subsequent density change of lattice occurs. Most important is the formation of ZrO_2, which causes a significant change in the volume. At the interface of α-$Zr(O)_C$ / ZrO_2, a movement of δx_6 due to oxygen diffusion produces an oxide layer of thickness $f.\delta x_6$ as shown in Fig.4. 'f' is the Pilling-Bedworth factor, which is the ratio of volume associated with one Zr atom in ZrO_2 and in the α-Zr(O) phase. It is given as 1.56. The difference (f - 1)δx pushes the ZrO_2 layer outwards with an expansion velocity V_{exp}.

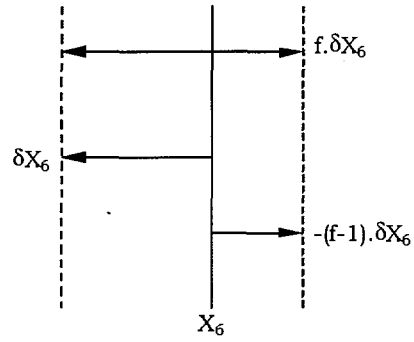

Fig.4 Change in layer thickness due to volumetric expansion

Velocity calculation at the boundaries :
The velocity at any interface because of only oxygen diffusion is given by

$$V^{\circ}_i = \frac{dx}{dt} = \left[-D_{i-1} \left.\frac{\partial C_{i-1}}{\partial r}\right|_{X_i} + D_i \left.\frac{\partial C_i}{\partial r}\right|_{X_i} \right] . \frac{1}{\Delta C_i} \qquad [5]$$

ΔC_i is calculated by subtracting the concentration at the left boundary of phase-'i' to that at the right boundary of phase-'i-1'. Experimentally, the interface '2' (Fig.2) is found to remain at the same location. Therefore, $V_2 = 0$ for any time.

The interface (U-Zr) / α-$Zr(O)_b$ shows an inverse concentration jump. The reason is due to low oxygen solubility in U-Zr phase and higher oxygen potential of α-$Zr(O)_b$. This give rise to instability of the interface and can not be simulated by mere oxygen diffusion process. Experimental observations [Hofmann, 1988] revealed that, the velocity (V_3) of the interface was found to be nearly 20% of the velocity of the inner phase boundary of α-$Zr(O)_a$ layer. Formation of ZrO_2, layer causes a significant change in the volume. Velocities at such interfaces is given by the following relation

$$V_i = \lambda V^{\circ}_i \qquad [6]$$

Where, $\ddot{e} = \dfrac{C_i - C_{i+1}}{(fC_i - C_{i+1})}$

MATERIAL PROPERTIES

The material properties like oxygen diffusion coefficient, phase boundary concentrations and metal densities are temperature dependent. Metal densities are required to obtain the volume expansion or contraction. The diffusion coefficient and phase boundary concentrations are obtained from literature (Hofmann, 1987)

It is reported by Denis (1991) and Hofmann (1988) that heating and cooling of the clad gives rise to stresses and strain in the outer oxide layer which leads to cracking and faster oxidation. Diffusion coefficient of ZrO_2 is given in Table – 1 as a function of both temperature and heating rate (Denis et al., 1991).

	Temperature (^{O}C)				
	T < 1350	1350 ≤ T < 1550	1550 ≤ T < 1750	1750 ≤ T < 1950	1950 ≤ T
V < 0.15	D	D	D	D	D
0.15 ≤ V < 0.9	D	2D	2D	2D	2D
0.15 ≤ V < 4.0	D	2D	6D	6D	6D
4.0 ≤ V < 9.0	D	2D	6D	12D	12D
9.0 ≤ V	D	2D	6D	12D	24D

$D = 1.29 \cdot 10^{-6} \exp(-125520/RT)$, m^2 /sec, V = heating rate, K/sec

Table-1: Diffusion coefficient of the layer ZrO_2

COMPUTER MODELLING

In order to solve the diffusion equation (Eq.2) in each layer, we have used the implicit finite difference method with grid sizes changing with layer width. Solution to this equation provides a distribution of oxygen in each layer. The interface movement is governed by the oxygen distribution in the adjacent layer.

Finite difference Equation Formulation :

The partial differential equations can be written in centered difference scheme as below :

$$\left.\frac{\partial C}{\partial r}\right|_i^{k+1} = \frac{C_{i+1}^{k+1} - C_{i-1}^{k+1}}{2\Delta r} \qquad [7(a)]$$

$$\left.\frac{\partial^2 C}{\partial r^2}\right|_i^{k+1} = \frac{C_{i+1}^{k+1} - 2C_i^{k+1} + C_{i-1}^{k+1}}{\Delta r^2} \qquad [7(b)]$$

$$\left.\frac{\partial C}{\partial t}\right|_i^{k} = \frac{C_i^{k+1} - C_i^{k}}{\Delta t} \qquad [7(c)]$$

subscript 'i' correspond to the space level and the superscript 'k' to the time level. Substituting above equations in Eq.1 and grouping the terms we have

$$C_i^{k+1} = \frac{C_i^k + (R - Z)C_{i-1}^{k+1} + (R + Z)C_{i+1}^{k+1}}{(1 + 2R)}$$

$$(R - Z)C_{i-1}^{k+1} + (R + Z)C_{i+1}^{k+1} - (1 + 2R)C_i^{k+1} = -C_i^k \qquad [7(d)]$$

where,

$$R = \frac{D\Delta t}{\Delta r^2} \text{ and } Z_i^k = \frac{D\Delta t}{2r_i\Delta t}$$

r_i is the radial distance of i^{th} node from the centre. Eq.7(d) is applied to each node in the domain. So we obtain a system of linear equations for each layer. They differ in the values of diffusion coefficient of oxygen 'D' and grid spacing Δr.
Eq.3 (Stefan's Equation) can be written in the difference formulation (Fig.5) as below,

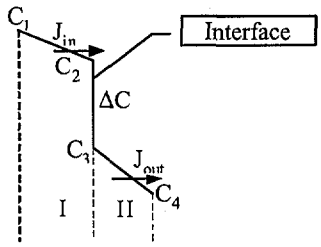

Fig 5 Computational scheme.

$$J_{in} = -D_I \frac{C_2 - C_1}{r_{33} - r_{22}} \quad \text{and} \quad J_{out} = -D_{II} \frac{C_4 - C_3}{r_{44} - r_{33}} \qquad [8]$$

velocity of an interface,

$$\frac{dx}{dt} = \frac{J_{in} - J_{out}}{C_2 - C_3} \qquad [9]$$

Meshing :
Due to the geometry of the fuel, cylindrical coordinate system is used in the formulation of finite difference equation. Each layer is divided into nodes with regular space interval of Δr. For a layer to exist it should have minimum thickness of 1μm. In order to minimize space and calculation time, mesh width is varied with time. Once the number of node changes for a layer, a concentration value is assumed for the new node and a new space convergence is carried out for the same previous time interval. The solution is then transferred to the next time interval.

Integration :
At each layer we obtain 'n' number of finite difference equations for 'n' no. of nodes. Equations can be written in the form [K][A] = [B]. At boundary of each layer following possible conditions are taken into account :

1. At the center of UO_2 fuel, we have the condition $\left.\frac{\partial C}{\partial r}\right|_{r=0} = 0$. Since oxygen atom diffuses from UO_2, the center-line oxygen concentration cannot be less than lower solubility limit of O_2 in UO_2.
2. Temperature dependent oxygen concentration at phase boundaries.

The matrix, thus obtained on applying the above boundary conditions are solved using Gauss Seidel iterative method. The interface movement (dx) is then calculated from the concentration gradient at the interface (Fig.5).

VERIFICATION TEST

Hofmann et al.[1988] performed out of pile UO_2/Zry reaction experiments in an (Ar + 25 vol% O_2) gas mixture in the high-temperature and high-pressure apparatus MONA. The test specimen is a short cladding tube filled with stoichiometric high-density UO_2 pellets. The specimens were 100 mm long with an outside diameter of 10.75 mm and a wall thickness of 0.72 mm. We have used the results of isothermal and tansient experiments performed by Hofmann et al.[1988] and Denis et al.[1991] separately. The input data used for the validation of the code is given in Table-2.

Clad Outer Diameter	5.32×10^{-3} m
Clad Inner Diameter	4.6×10^{-3} m
UO_2 Outer Diameter	4.6×10^{-3} m
Computational Time Interval	0.01 sec
Initial Temperature (^{O}C)	$1000^{O}C$
Initial oxygen conc. In UO_2 pellet at time, t = 0	1.298 g/cm^3
Initial oxygen conc. In clad at time, t = 0	8.5×10^{-3} g/cm^3

Table-2: Input

APPLICATION TO INDIAN PHWR FUEL PIN

The simultaneous interaction of pellet - clad - steam has been simulated for Indian PHWR fuel pin configuration to assess the fuel integrity under postulated severe accidental condition. The input data used for the calculation are given in Table-3. The temperature transient has been obtained from the RELAP4/MOD6 simulation of a 200% Header break along with failure of ECCS in PHWR system. Two sets of transient data were obtained (i) maximum powered channel (hot-channel) connected to the broken loop and (ii) maximum powered channel connected to unbroken loop (Fig.6).

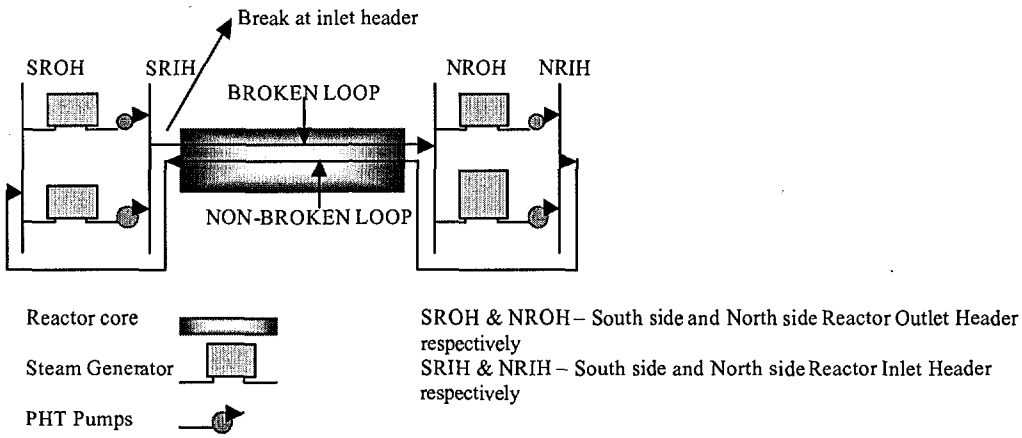

Fig.6 PWHR System simulated by RELAP4 / MOD6

Clad Outer Diameter	15.29×10^{-3} m
Clad Inner Diameter	14.47×10^{-3} m
UO_2 Outer Diameter	14.47×10^{-3} m
Computational Time Interval	0.01 sec
Initial Temperature (^{O}C)	$850^{O}C$
Initial oxygen conc. in UO_2 pellet at time, t = 0	1.298 g/cm^3
Initial oxygen conc. in clad at time, t = 0	8.5×10^{-3} g/cm^3

Table-3: Input

At temperature above $900^{O}C$, the fuel pins are found to balloon and contact each other, causing a steam starvation condition at contact points. So the steam condition would vary along the circumference of the clad. Since the code is 1D, the interaction for steam availability and steam non-availability condition has been simulated separately. The external interaction of clad-steam starts at $850^{O}C$ and internal at $1000^{O}C$ when sufficient contact exists between fuel and clad.

RESULTS AND DISCUSSION

Verification :

Results from the code simulations were obtained for isothermal temperatures $1100^{O}C$ and $1200^{O}C$ and transient temperature conditions of heat up and cool down rate 5 K/s and 10 K/s. The layer thicknesses calculated were compared with the experimental data published by (i) Hofmann et al.[1988] and (ii) Denis et al. [1991]. In the isothermal plots (Fig.7 and 8), X-axis representing the time scale and Y axis the distance of each layer from UO_2/α-Zr(O) interface. Fig.9 and Fig.10 compare the transient results with Denis et al. experiment data. In spite of the simplifications such as neglecting the effect of uranium and zirconium lattice movement, the layer formation and growths were reasonably well predicted by the code.

Application to Indian PHWR :

The plots Fig.11, Fig.12, Fig.13 and Fig.14 are obtained for PHWR fuel pins at different transient conditions. It can be observed that steam starvation would basically accelerate the internal oxidation and the heating rate greatly influences the layer growth. The thickness of α-Zr(O) and ZrO_2 produced at internal and external boundary would determine the fuel integrity on cool down. For the case of hot channel broken loop with steam availability condition, at $1200^{O}C$ the ZrO_2 thickness is found to be 40μm which is below the 0.17 times of Zircaloy clad thickness fuel integrity criterion. The average oxygen content is about 37 kg / m^3 (0.57 wt%) in unoxidized β-Zircaloy, which is more than 0.5 wt% of the oxygen criteria.

NOMENCLATURE

C	-	Oxygen concentration, kg / m^3
D	-	Diffusion coefficient, m^2 / s
f	-	Pilling-Bedworth factor
J	-	Flux, kg / m^2-s
R	-	Universal Gas constant, 8.314 J / K-mol
T	-	Temperature, K
t	-	Time, sec.
V	-	Velocity, m / s
V^O	-	Velocity due to oxygen diffusion only
x	-	Radial interface position, m
r	-	Radial distance from pellet center, m

Subscript:

i	-	Interface number
in	-	In flux
out	-	Out flux
exp	-	Expansion

REFERENCES

[1] Cronenberg, A.W., El-Genk, M.S., 1978, "An assessment of Oxygen Diffusion during UO_2-Zircaloy Interaction", J. of Nucl. Mat. 78, 390-407.

[2] Denis, A., Garcia, E.A., 1983, "A model to describe the interaction between UO_2 and zircaloy in the temperature range 1000 to 1700^{O}C", J. of Nucl. Mat. 116, 44 – 54.

[3] Denis, A., Garcia, E.A., 1991, "Simulation with the HITO code of the interaction of Zircaloy with Uranium dioxide and steam at high temperature", J. of Nucl. Mat. 185, 96-113.

[4] Fischer, S. R., et. al, 1978, "RELAP4/MOD6: A Computer Program for Transient Thermal-Hydraulic Analysis of Nuclear Reactors and Related Systems, User's Manual," Technical Report no. CDAP TR003, INEL, USA

[5] Grossman, L.N., Rooney, D.M., 1965, Report GEAP 4679.

[6] Hofmann, P. et al., 1987, "New determination of the UO_2/Zircaloy reaction kinetics and calculation of the oxygen diffusion coefficients", Report No : kfk 4253.

[7] Hofmann, P. et al., 1988, "Chemical interactions of zircaloy – 4 tubing with UO_2 fuel and oxygen at temperature between 900 and 2000^{O}C", (experiments and PECLOX code), Report No : kfk 4422.

[8] Hofmann, P., Kerwin-Peck, D.K., 1984, "UO_2/Zry Chemical interaction under Isothermal and Transient Temperature Conditions", J. of Nucl. Mat., 124, 80-105.

[9] Hofmann, P., Politis, C., 1979, J. Nucl. Mat, 87, 375.

[10] Mallett, M.W. et al. , 1957, Report BMI 1210.

[11] Olander, D.R., 1983, "The UO_2/Zircaloy-Chemical Interactions", J. of Nucl. Mat. 116, 44-54.

[12] Politis, C., KFK 2167, Kernforschungszentrum Karlsruhe, Karlsruhe, West Germany, 1975.

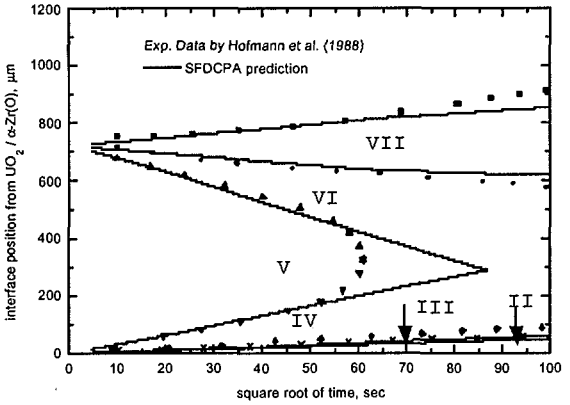

Fig.7 Various interface position for isothermal experiments at 1100°C and comparison with SFDCPA prediction.

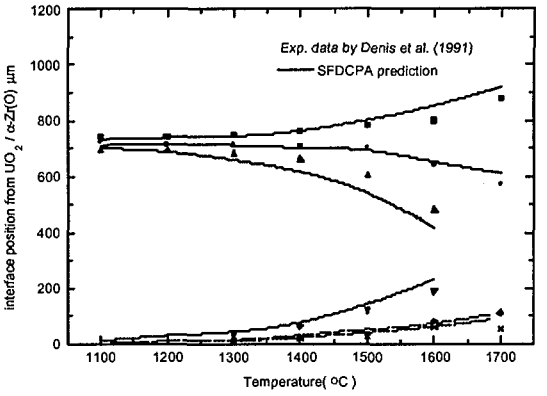

Fig.10 Various interface position for transient experiments at 10K/s and comparison with SFDCPA prediction.

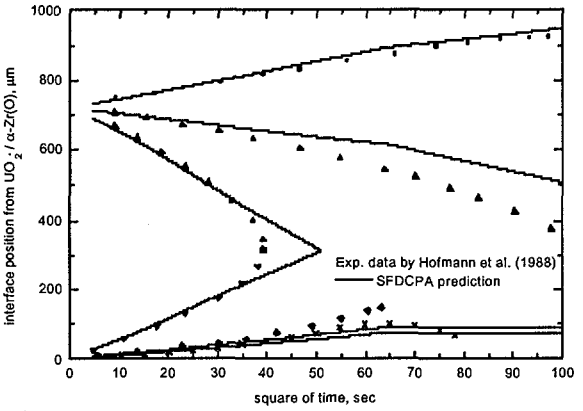

Fig.8 Various interface position for isothermal experiments at 1200°C and comparison with SFDCPA prediction.

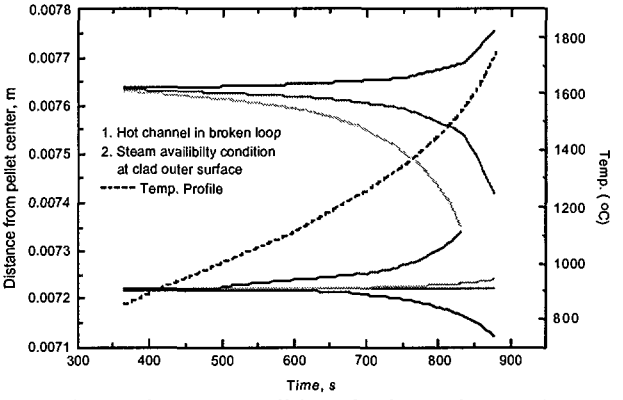

Fig. 11 Fuel pin condition in hot channel broken loop with steam availability at clad outer surface.

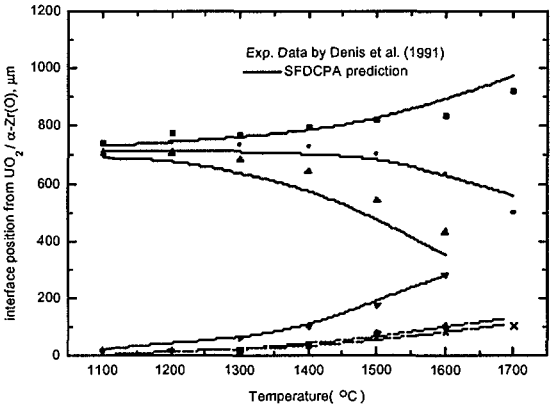

Fig.9 Various interface position for transient experiments at 5K/s and comparison with SFDCPA prediction.

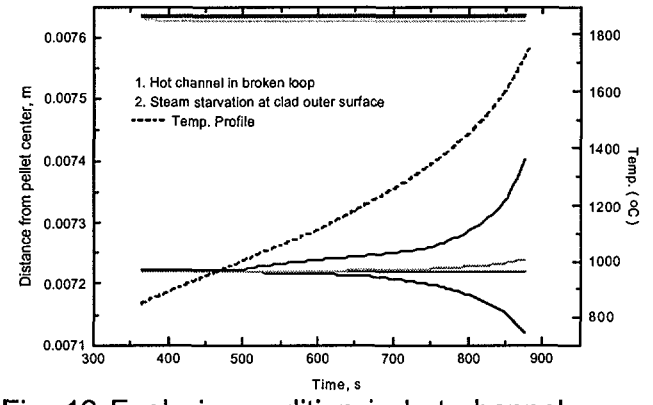

Fig. 12 Fuel pin condition in hot channel broken loop during steam starvation condition.

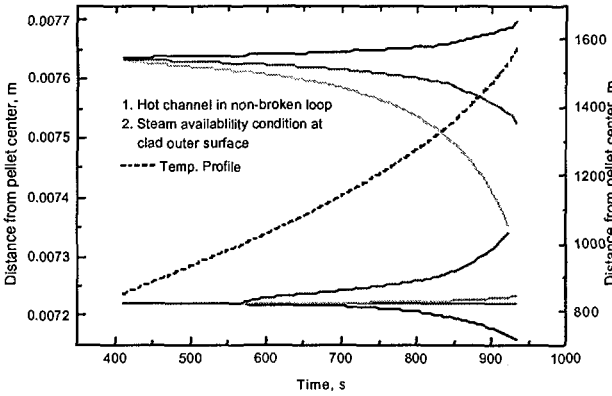

Fig. 13 Fuel pin condition in hot channel non-broken loop with steam availability at clad outer surface.

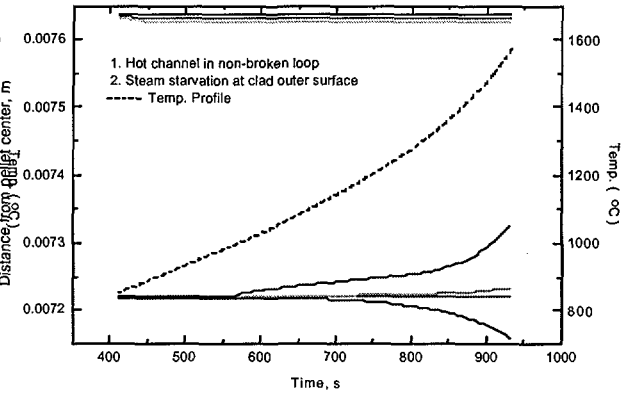

Fig.14 Fuel pin condition in hot channel non-broken loop during steam starvation condition.